# Structure and Dynamics in Alkanethiolate Monolayers Self-Assembled on Gold Nanoparticles: A DSC, FT-IR, and Deuterium NMR Study

**Antonella Badia,† Louis Cuccia, Linette Demers, Fred Morin, and R. Bruce Lennox***

*Contribution from the Department of Chemistry, McGill University, 801 Sherbrooke Street West, Montreal, Quebec, Canada H3A 2K6*

*Received October 14, 1996*[⊗]

**Abstract:** Gold nanoparticles, *ca*. 30 Å in diameter, have been derivatized with specifically deuterated (position 1 and positions 10 to 13) and perdeuterated (positions 2 to 18) octadecanethiols ($C_{18}SH$). The phase behavior of the octadecanethiolate monolayers chemisorbed onto the colloidal gold surface was characterized by differential scanning calorimetry (DSC). The DSC thermograms show that the $C_{18}SH$-derivatized Au nanoparticles undergo distinct phase transitions which can be associated with the reversible disordering of the alkyl chains. Despite the highly curved geometry of these Au particles, there is a remarkable degree of conformational order in the alkanethiolate chains and the thermotropic behavior of the thiol-modified gold nanoparticles is very similar to that of conventional, planar self-assembled monolayers. Both the peak maximum temperature and the enthalpy associated with the DSC transition strongly parallel those of the gel-to-liquid crystalline transition of *n*-diacylphosphatidylcholine lipid bilayer membranes of equivalent chain length. Restricted chain mobility due to covalent bonding of the sulfur head group to the gold surface does not affect the cooperativity of the transition in terms of the transition temperature and enthalpy. Local chain ordering and dynamics in the deuterated $C_{18}S$/Au nanoparticles have been probed using variable-temperature solid-state deuterium NMR spectroscopy and transmission FT-IR spectroscopy. The temperature dependence of the symmetric $CD_2$ stretching frequency has confirmed that the DSC-detected phase transition involves a thermally-induced change from a predominantly all-*trans* conformation to a chain disordered state. A comparison of the thermal behavior of $d_{35}$-$C_{18}S$/Au and *10,10,11,11,12,12,13,13-*$d_8$-$C_{18}S$/Au shows that disordering originates in the chain terminus region and propagates toward the middle of the chain as the temperature increases. Studies of *1,1-*$d_2$-$C_{18}S$/Au show that the disorder does not extend to the tethered sulfur head group. Deuterium NMR spectroscopy specifically establishes that chain melting arises from an increased frequency of *gauche* bonds in the alkanethiolate chains. The $^2H$ NMR line shapes further indicate that the tethered alkanethiolate chains are undergoing rapid *trans-gauche* bond isomerization and axial chain rotation.

## Introduction

We have recently investigated the phase properties of self-assembled alkanethiolate (RS) monolayers on metal surfaces *via* the synthesis of alkanethiol-stabilized gold clusters.[1,2] This system was chosen because of its unique potential to serve as a highly dispersed analogue to self-assembled monolayers (SAMs) formed on planar metal surfaces. Transmission electron microscopy established that the nanoparticles have average Au core diameters ranging from 20 to 30 Å, with a typical size polydispersity of 30%.[1] Elemental analysis results for an octadecanethiol-derivatized Au cluster showed that the gold core (median diameter of 22.4 Å), modeled as a sphere, contains ∼346 Au atoms and ∼102 octadecanethiolate chains, resulting in a surface Au-to-thiolate ratio of 2.2.[1,3] This leads to a higher alkanethiolate surface density on the nanoparticles (15.4 Å$^2$/molecule) as compared to the flat Au(111) surface widely used for thiol self-assembly (21.4 Å$^2$/molecule).[4] These alkanethiol-derivatized Au nanoparticles are isolated as black solids whose texture ranges from a wax to fine crystals, depending on the alkane chain length. They are air-stable and soluble in chloroform, toluene, hexanes, and other nonpolar solvents. The solvent can be evaporated, and the particles can be repeatedly redissolved in organic solvent without metallization occurring. Most importantly, the high surface area of these nanoparticles (*i.e. ca.* 100 m$^2$/g) offers access to much larger quantities of the monolayer surfactant, rendering the self-assembled thiol monolayer amenable to structural characterization by techniques conventionally used for bulk materials. NMR spectroscopy (both solution[1,2,5,6] and solid state[2]), transmission FT-IR spectroscopy,[1,7−9] and differential scanning calorimetry[1,5] are of particular note.

* Author to whom correspondence should be addressed.

† Present address: Max-Planck-Institut für Polymerforschung, Postfach 3148, D-55021 Mainz (FRG).

⊗ Abstract published in *Advance ACS Abstracts,* February 15, 1997.

(1) Badia, A.; Singh, S.; Demers, L.; Cuccia, L.; Brown, G. R.; Lennox, R. B. *Chem. Eur. J.* **1996**, *2*, 359−363.

(2) Badia, A.; Gao, W.; Singh, S.; Demers, L.; Cuccia, L.; Reven, L. *Langmuir* **1996**, *12*, 1262−1269.

(3) If these $C_{18}S$/Au nanoparticles are modeled as truncated octahedra containing 459 Au atoms (so-called Magic number) in the Au core,[16] the elemental analysis results yield ∼136 $C_{18}S$ chains per particle and hence a surface Au-to-thiolate ratio of 1.8.

(4) Camillone, N.; Chidsey, C. E. D.; Liu, G.; Scoles, G. *J. Chem. Phys.* **1993**, *98*, 4234−4245.

(5) Terrill, R. H.; Postlethwaite, A.; Chen, C.-h.; Poon, C.-D.; Terzis, A.; Chen, A.; Hutchison, J. E.; Clark, M. R.; Wignall, G.; Londono, J. D.; Superfine, R.; Falvo, M.; Johnson, C. S., Jr.; Samulski, E. T.; Murray, R. W. *J. Am. Chem. Soc.* **1995**, *117*, 12537−12548.

(6) Hostetler, M. J.; Green, S. J.; Stokes, J. J.; Murray, R. W. *J. Am. Chem. Soc.* **1996**, *118*, 4212−4213.

(7) Brust, M.; Walker, M.; Bethell, D.; Schiffrin, D. J.; Whyman, R. *J. Chem. Soc., Chem. Commun.* **1994**, 801−802.

(8) Brust, M.; Fink, J.; Bethell, D.; Schiffrin, D. J.; Kiely, C. *J. Chem. Soc., Chem. Commun.* **1995**, 1655−1656.

(9) Hostetler, M. J.; Stokes, J. J.; Murray, R. W. *Langmuir* **1996**, *12*, 3604−3612.

S0002-7863(96)03571-8 CCC: $14.00 

We find that SAMs on colloidal Au particles show strong parallels to the monolayers formed at planar surfaces,[1,9,10] given the excellent correspondence in chain ordering/disordering phenomena in these two systems. The CH stretching vibrations in the FT-IR spectra of RS/Au nanoparticles (where R = $C_8$−$C_{20}$) indicate that for R ≥ $C_{16}$, the alkyl chain exists predominantly in an extended, all-*trans* conformation at 25 °C.[1,11] Moreover, a recent, detailed FT-IR study by Hostetler *et al.*[9] reports that analogous to conventional RS/Au SAMs, long chain RSHs self-assembled on the Au nanoparticles possess a high percentage of end-*gauche* defects, no detectable internal *gauche* conformers, and a small amount of near surface *gauche* defects. Solid-state $^{13}$C NMR spectroscopy further reveals the coexistence of motionally restricted all-*trans* chains with a smaller population of liquid-like conformationally disordered chains in $C_{18}$S/Au at 25 °C.[2] Calorimetry,[1,5] variable-temperature FT-IR spectroscopy,[1] and solid-state $^{13}$C NMR studies[1,2] have established that a chain melting transition occurs in these alkylated metal colloids. The transition temperature associated with each chain (for R = $C_{12}$−$C_{20}$) closely parallels those found in electrochemical studies of planar RS/Au SAMs,[10] X-ray diffraction studies of fatty acid Langmuir−Blodgett monolayer films,[12] and calorimetry studies of phospholipid bilayer membranes.[13] Melting transitions are highly sensitive to the degree of chain organization. That the thermotropic behavior of the RS/Au nanoparticles is very similar to that of highly ordered, 2D self-assembled systems tells us that there is a surprisingly high degree of chain conformational order in these coated colloids. Differences between the strictly planar and colloid systems do arise however due to the high radius of curvature of the nanoparticles and the presence of single-crystal facets on the surface.[5,8,14−18] In planar RS/Au SAMs, the alkyl chain packing density and organization are largely dictated by the underlying metal lattice and extensive, chain−chain van der Waals interactions.[4,19] How chain ordering arises in the RS/Au colloids is not immediately apparent given that the length of the tethered RS chain and the Au core diameter are similar and the relation between the extended chain conformation and the highly curved geometry of these particles. Transmission electron microscopy of (sub)monolayer films,[1,15,16] powder X-ray diffraction of thick film samples,[15,16,20] and density measurements of the solid material[5] reveal that adjacent Au particles are separated by approximately one chain length, and not by the expected two chain lengths. Based on this observation, we proposed that long range ordering arises from an interdigitation of *chain domains* on neighboring particles.[1] An alternative packing configuration, involving the interdigitation of individual chains,[5] is not likely given the large ratio of chain end area to Au−S head group area of 14:1.[1] Recent molecular dynamics (MD) simulations of dodecanethiol-derivatized Au nanoparticles support our chain packing model.[15,17] More specifically, the MD simulations predict that the dodecanethiolate monolayer forms oriented molecular *domains* or "*bundles*" of conformationally ordered chains at temperatures below the phase transition temperature. Furthermore, the $C_{12}$S/Au nanoparticles in these simulations assemble into 3D superlattices through the "interlocking" of molecular bundles on neighboring particles and not *via* the interdigitation of individual chains.[17]

Despite the rapid advances made in characterizing these interesting materials, several important issues (such as chain dynamics, structure, and orientation) have not been directly addressed to date. To this end, we now report the use of deuterium labeling to probe both the local ordering and chain dynamics of alkanethiols adsorbed to the surface of these gold nanoparticles. Solid-state deuterium NMR spectroscopy, in conjunction with FT-IR spectroscopy and differential scanning calorimetry (DSC), is used to study the thermodynamics of RSH-derivatized Au nanoparticles. In the past, solid-state $^2$H NMR has been extensively used to probe conformational order and molecular motion in lipid membranes,[21−24] spherical supported lipid bilayers,[25,26] rigid-rod polymers with alkyl side groups,[27−29] alkylammonium layer-structure compounds,[30] and alkylsilyl-modified silica gel chromatographic stationary phases.[31,32] Solid-state $^2$H NMR spectroscopy offers distinct advantages over $^{13}$C and $^1$H NMR for probing the structure and dynamics of ordered systems. The peaks observed in $^2$H NMR originate from the nuclear quadrupole coupling of the deuteron with the electric field gradient of the C−$^2$H $\sigma$-bond. An axially symmetric quadrupolar interaction dominates the $^2$H NMR spectrum so that the line shapes are simple and solely dependent upon the amplitude and symmetry of the molecular motions. The peak shapes reflect intramolecular dynamics and there are no complex contributions from chemical shift anisotropy and heteronuclear dipolar interactions which greatly increase the complexity of $^{13}$C and $^1$H NMR spectra in regards to analyzing motional phenomena. Furthermore, since the relaxation of the $^2$H nucleus is dominated by the quadrupolar interaction, there is no need to establish relaxation mechanisms.[23,32−34] More importantly, the low natural abundance of deuterium (*i.e.* 0.015%) eliminates background contributions from unlabeled

(10) Badia, A.; Back, R.; Lennox, R. B. *Angew. Chem., Int. Ed. Engl.* **1994**, *33*, 2332−2335.
(11) Demers, L.; Badia, A.; Lennox, R. B. Unpublished results.
(12) Riegler, J. E. *J. Phys. Chem.* **1989**, *93*, 6457−6480.
(13) Marsh, D. *Handbook of Lipid Bilayer Membranes*; CRC Press: Boca Raton, 1991, pp 135−150.
(14) Leff, D. V.; Ohara, P. C.; Heath, J. R.; Gelbart, W. M. *J. Phys. Chem.* **1995**, *99*, 7036−7041.
(15) Whetten, R. L.; Khoury, J. T.; Alvarez, M. M.; Murthy, S.; Vezmar, I.; Wang, Z. L.; Cleveland, C.; Luedtke, W. D.; Landman, U. In *Proceedings of the NATO Advanced Research Workshop on "The Chemical Physics of Fullerenes 10 (and 5) Years Later"*; Kluwer Academic Publishers: Varenna, Italy, 1995; pp 475−490.
(16) Whetten, R. L.; Khoury, J. T.; Alvarez, M. M.; Murthy, S.; Vezmar, I.; Wang, Z. L.; Stephens, P. W.; Cleveland, C. C.; Luedtke, W. D.; Landman, U. *Adv. Mater.* **1996**, *8*, 433−437.
(17) Luedtke, W. D.; Landman, U. *J. Phys. Chem.* **1996**, *100*, 13323−13329.
(18) Lebuis, A. M., X-ray Diffraction Facility, Department of Chemistry, McGill University, Dec. 1996, personal communication.
(19) Dubois, L. H.; Nuzzo, R. G. *Annu. Rev. Phys. Chem.* **1992**, *43*, 437−463.
(20) Lebuis, A. M., X-ray Diffraction Facility, Department of Chemistry, McGill University, Nov. 1995, personal communication.
(21) Griffin, R. G. *Methods Enzymol.* **1981**, *72*, 108.
(22) Davis, J. H. *Biochim. Biophys. Acta* **1983**, *737*, 117−171
(23) Smith, R. L.; Oldfield, E. *Science* **1984**, *225*, 280−288.
(24) Blume, A.; Hubner, W.; Muller, M.; Bauerle, H. D. *Ber. Bunsenges. Phys. Chem.* **1989**, *93*, 964−973.
(25) Naumann, C.; Brumm, T.; Bayerl, T. M. *Biophys. J.* **1992**, *62*, 1314−1319.
(26) Bayerl, T. M.; Bloom, M. *Biophys. J.* **1990**, *58*, 357−362.
(27) Spiess, H. W. *Ber. Bunsenges. Phys. Chem.* **1993**, *97*, 1294−1305.
(28) Kricheldorf, H. R.; Wutz, C.; Probst, N.; Domschke, A.; Gurau, M. In *Multidimensional Spectroscopy of Polymers: Vibrational, NMR, and Fluorescence Techniques*; Urban, M. W., Provder, T., Eds.; American Chemical Society: Washington, DC, 1995; pp 311−332.
(29) van Genderen, M. H. P.; Pfaadt, M.; Moller, C.; Valiyaveettil, S.; Spiess, H. W. *J. Am. Chem. Soc.* **1996**, *118*, 3661−3665.
(30) Jurga, S.; Macho, V.; Huser, B.; Spiess, H. W. *Z. Phys. B−Condensed Matter* **1991**, *84*, 43−49.
(31) Kelusky, E. C.; Fyfe, C. A. *J. Am. Chem. Soc.* **1986**, *108*, 1746−1749.
(32) Ziegler, R. C.; Maciel, G. E. *J. Am. Chem. Soc.* **1991**, *113*, 6349−6358.
(33) Jelinski, L. W.; Dumais, J. J.; Engel, A. K. *Macromolecules* **1983**, *16*, 492−496.
(34) Fyfe, C. A. In *Solid State NMR for Chemists;* C.F.C. Press: Guelph, Canada, 1983; pp 73−137.

material so that the dynamics of a single chain position or residue can be exclusively observed in selectively labeled molecules.

Quadrupolar splitting in $^2$H NMR is especially sensitive to motions and orientations at different positions in a molecule. For the $^2$H nucleus with spin $I = 1$ and an asymmetry parameter $\eta = 0$ for the C$-^2$H bond, the allowed energy transitions are $-1 \leftrightarrow 0$ and $0 \leftrightarrow 1$, giving rise to a doublet in the NMR spectrum with a peak separation given by

$$\Delta\nu_Q = {}^3/_4(e^2qQ/h)(3\cos^2\theta - 1) \quad (1)$$

where $\Delta\nu_Q$ is the quadrupolar splitting or peak separation in frequency units, $(e^2qQ/h)$ is the quadrupolar coupling constant (168 kHz for an aliphatic sp$^3$ C$-^2$H bond), and $\theta$ is the angle between the principal axis of the electric field tensor of the $^2$H nucleus and the magnetic field, $H_o$.[23,34] For a rigid polycrystalline solid, all values of $\theta$ are possible and a so-called rigid powder pattern or Pake pattern is obtained. In this case, the separation between the peak maxima ($\theta = 90°$) is *ca*. 130 kHz and the separation between the steps at the wings ($\theta = 0°$) is twice this value.[23,34] In the case of lipid membranes, organic thin films, and rigid-rod polymers with flexible side chains, there is considerable intramolecular motion due to such processes as methyl group rotation, *trans-gauche* bond isomerization, axial rotation, lateral diffusion of molecules, or flipping of a phenyl ring about its $C_2$ axis. Molecular motions that have correlation times of *ca*. $10^{-7}-10^{-4}$ s[23,33] can be studied by $^2$H NMR, a much longer time scale than most other spectroscopic techniques. Motions that are slow on the NMR time scale are expected to have a negligible influence on the $^2$H NMR spectrum. Fast motions ($t \ll 10^{-6}$ s), on the other hand, cause the $(3\cos^2\theta - 1)$ term in eq 1 to be averaged with time, resulting in a decrease of the quadrupolar splitting and/or changes in the peak line shape.[23,34] Thus, in most cases, the $^2$H NMR spectral line shapes and the spin$-$lattice ($T_1$) relaxation times provide incisive information regarding molecular orientation as well as the type and the rate of motion that a particular $^2$H-labeled site is undergoing.[23,34] For this reason, FT-IR and $^2$H NMR spectroscopy can give complementary information on the structure and dynamics of $^2$H-labeled systems, given that FT-IR spectroscopy probes a time scale which is less than $10^{-10}$ s.[35]

In this study, *n*-octadecanethiols deuterated at different positions along the alkyl chain were used to derivatize the surface of Au nanoparticles. The molecules synthesized include the following: $\mathbf{CD_3(CD_2)_{16}}CH_2SH$ (positions 2 to 18 deuterated), $CH_3(CH_2)_{16}\mathbf{CD_2}SH$ (position 1 deuterated), and $CH_3(CH_2)_4\mathbf{CD_2CD_2CD_2CD_2}(CH_2)_9SH$ (positions 10 to 13 deuterated).

Solid-state $^2$H NMR spectroscopy is used to show that the DSC-detected phase transition is a thermally-induced chain melting process. FT-IR spectroscopy establishes that the chain melting begins at the chain terminus and propagates toward the middle of the chain with increasing temperature. The excellent correspondence observed between the thermal properties of RSH SAMs on planar and colloidal Au surfaces suggests that the nanoparticle solid-state NMR results are applicable to conventional SAMs.

(35) Bloom, M.; Thewalt, J. *Chem. Phys. Lipids* **1994**, *73*, 27−38.

(36) $C_{14}S$/Au nanoparticles synthesized using a 3:1 mole ratio of $AuCl_4^-$ to $C_{14}H_{29}SH$ had a mean diameter of $33 \pm 7$ Å. A partial elemental analysis (Galbraith Laboratories) yielded 73.51% Au and 3.21% S, resulting in a surface Au-to-thiol ratio of 2.1.

## Experimental Section

**Materials.** $d_{35}$-Stearic acid (98 atom % D) and deuterium gas (99.99%) were purchased from Cambridge Isotope Laboratories, Inc. (Andover, MA). 10,12-Octadecadiynoic acid was obtained from Farchan Laboratories, Inc. (Gainesville, FL). Stearic acid (lab-grade), from Anachemia Chemicals Ltd. (Montreal, Canada), was recrystallized from hexanes before use. *n*-Octadecanethiol (98%, Aldrich Chemical Co., Milwaukee, WI) was recrystallized three times from ethanol. Tris-(triphenylphosphine)rhodium(I) chloride (Wilkinson's catalyst), lithium aluminum hydride, lithium aluminum deuteride (98 atom % D), hydrogen tetrachloroaurate(III) trihydrate, and tetraoctylammonium bromide were all purchased from Aldrich. Sodium thiosulfate was from A&C American Chemicals Ltd. (Montreal, Canada) and 48% HBr was from Fluka Corp. (Ronkonkoma, NY).

***d*$_{35}$-Octadecanethiol.** $d_{35}$-Stearic acid (1.10 g, 3.45 mmol) was dissolved in 60 mL of dry THF. This solution was added *via* a dropping funnel to a three-neck round-bottom flask equipped with a reflux condenser and a calcium carbonate drying tube and containing $LiAlH_4$ (1.04 g, 27.5 mmol) dissolved in 125 mL of dry THF. The reaction mixture was refluxed for *ca*. 12 h. The reaction vessel was cooled in an ice bath and distilled water was carefully added dropwise to the reaction mixture to destroy the residual $LiAlH_4$. A 4-mL aliquot of 6 N HCl solution was added and reflux was continued for an additional 12 h. Hexanes (100 mL) were added with stirring to the cooled reaction mixture. The remaining white precipitate was removed by filtration at this stage and the mixture was poured into a separatory funnel. The organic layer was separated from the aqueous layer. The aqueous phase was further extracted with 2 x 50 mL of hexanes. The combined organic extracts were washed with 2 × 100 mL of distilled water and then dried over anhydrous magnesium sulfate. The solvent was removed by rotary evaporation to yield 0.980 g (93%) of $d_{35}$-octadecanol (*i.e.* $CD_3(CD_2)_{16}CH_2OH$).

The perdeuterated octadecanol (0.980 g, 3.21 mmol) was added to a mixture of 50 mL of 48% HBr and 100 $\mu$L of concentrated $H_2SO_4$. The mixture was refluxed for 8 h. The HBr mixture was diluted with 25 mL of distilled water and 50 mL of hexanes was added with stirring. The hexanes phase was separated from the aqueous HBr phase, and then the HBr phase was further extracted with 2 × 50 mL of hexanes. The hexanes extracts were pooled together, washed with 2 × 75 mL of water, and dried over anhydrous magnesium sulfate. The solvent was removed by rotary evaporation and the residue purified by column chromatography (silica gel, *n*-hexane) to yield 0.986 g (84%) of $d_{35}$-octadecyl bromide.

The octadecyl bromide (0.980 g, 2.66 mmol) was dispersed in 50 mL of absolute ethanol. A solution of $Na_2S_2O_3{\cdot}5H_20$ (0.660 g, 2.66 mmol) in 10 mL of water was added to the octadecyl bromide and the reaction was refluxed for 6 h. The resulting Bunte salt was hydrolyzed with HCl (9.0 mL of 6 N HCl) by refluxing for 4 h under a nitrogen atmosphere. The cooled reaction mixture was poured with stirring into a two-phase mixture of 10 mL of distilled water and 25 mL of hexanes. The organic layer was separated from the aqueous layer, and the aqueous phase was then further extracted with 2 × 25 mL of hexanes. The combined hexanes extracts were washed with 2 × 35 mL of water and dried over anhydrous magnesium sulfate. The solvent was removed by rotary evaporation and the residue was recrystallized from ethanol to yield pure $d_{35}$-octadecanethiol (0.768 g, 90%). TLC (silica gel, *n*-hexane): $R_f$ 0.7; $^1$H NMR (499.84 MHz, $CDCl_3$) $\delta$ 2.52 (s, C$\mathbf{H}_2$SH); $^2$H NMR (76.73 MHz, $CHCl_3$) $\delta$ 0.83 (s, 3D, $CD_3$), 1.19 (s, 30D, $CD_3(C\mathbf{D}_2)_{15}$), 1.53 (s, 2D $CD_2CH_2SH$). MS (EI) *m/z* 321 $[M]^{\bullet+}$.

***1,1-d*$_2$-Octadecanethiol.** Stearic acid (2.00 g, 7.03 mmol) was converted to *1,1-d*$_2$-octadecanol (1.78 g, 93%) by reduction with $LiAlD_4$ as described above. Bromination followed by Bunte salt formation and hydrolysis using the procedures previously described yielded *1,1-d*$_2$-octadecanethiol (1.36 g, 67% with respect to stearic acid). TLC (silica gel, *n*-hexane): $R_f$ 0.7; $^1$H NMR (499.84 MHz, $CDCl_3$) $\delta$ 1.59 (t, 2H, C$\mathbf{H}_2$CD$_2$SH), 1.37 (m, 2H, C$\mathbf{H}_2$CH$_2$CD$_2$SH), 1.26 (s, 28H, $CH_3(C\mathbf{H}_2)_{14}$), 0.88 (t, 3H, $CH_3$); $^2$H NMR (76.73 MHz, $CHCl_3$) $\delta$ 2.49 (s, $CD_2SH$); MS (EI) *m/z* 288 $[M]^{\bullet+}$.

***10,10,11,11,12,12,13,13-d*$_8$-Octadecanethiol.** 10,12-Octadecadiynoic acid (1.00 g, 3.62 mmol) was dissolved in 10 mL of freshly distilled, argon saturated THF in a pressure reactor. Wilkinson's catalyst (100

mg) was added and the reactor was evacuated and flushed with argon three times. The reactor was then flushed with $D_2$ gas and filled to a pressure of 1 psi. The reaction mixture was stirred for ~19 h after which the reactor was refilled with additional $D_2$ gas. The reaction mixture was stirred for an additional 3 days. The solvent was removed by rotary evaporation and the residue chromatographed (silica gel, 80:20 (v/v) hexanes−ethyl acetate). Recrystallization from hexanes yielded pure *10,10,11,11,12,12,13,13-*$d_8$-octadecanoic acid (0.495 g, 47%). mp 67−69 °C; $^1$H NMR (499.84 MHz, $CDCl_3$) $\delta$ 2.35 (t, 2H, C**H**$_2$COOH), 1.63 (m, 2H, C**H**$_2$CH$_2$COOH), 1.25 (s, 20H, CH$_3$(C**H**$_2$)$_4$(CD$_2$)$_4$(C**H**$_2$)$_6$CH$_2$CH$_2$COOH), 0.88 (t, 3H, CH$_3$); $^2$H NMR (76.73 MHz, $CHCl_3$) $\delta$ 0.93 (s, (CD$_2$)$_4$).

*10,10,11,11,12,12,13,13-*$d_8$-Octadecanoic acid (0.485 g, 1.66 mmol) was reduced to the alcohol (0.364 g, 79%) using $LiAlH_4$ as described previously. Bromination with 48% HBr followed by Bunte salt formation and hydrolysis yielded *10,10,11,11,12,12,13,13-*$d_8$-octadecanethiol (0.268 g, 70% with respect to $d_8$-octadecanol). TLC (silica gel, *n*-hexane): $R_f$ 0.7; $^1$H NMR (499.84 MHz, $CDCl_3$) $\delta$ 2.51 (t, 2H, C**H**$_2$SH), 1.59 (m, 2H, C**H**$_2$CH$_2$SH), 1.37 (m, 2H, C**H**$_2$CH$_2$CH$_2$SH), 1.25 (s, 20H, CH$_3$(C**H**$_2$)$_4$(CD$_2$)$_4$(C**H**$_2$)$_6$CH$_2$CH$_2$CH$_2$SH), 0.88 (t, 3H, CH$_3$); MS (EI) *m/z* 294 $[M]^{\bullet+}$

**$C_{18}$SH-Derivatized Gold Nanoparticles.** Gold nanoparticles derivatized with *10,10,11,11,12,12,13,13-*$d_8$-octadecanethiol, *1,1-*$d_2$-octadecanethiol, and $d_{35}$-octadecanethiol were prepared following the method of Brust *et al.*[1,7] The syntheses were carried out using 1.8 mmol of $HAuCl_4 \cdot 3H_2O$ and a modified $AuCl_4^-$:$C_{18}$SH mole ratio of 3:1, instead of 1:1.[7] The 3:1 $AuCl_4^-$:RSH ratio was used because it produces fully covered Au nanoparticles (~30 Å in diameter) and eliminates the exhaustive (and exhausting!) washing/extraction process required to remove the large amounts of residual thiol and disulfide present in the original preparation.[1,36] For the synthesis of Au nanoparticles coated with *10,10,11,11,12,12,13,13-*$d_8$-octadecanethiol, only one-third of the octadecanethiol surfactant molecules were deuterated. For the other syntheses, the deuterated octadecanethiols were used undiluted. The $C_{18}$S/Au colloids were purified as described previously and dried under vacuum.[1] Complete removal of unbound thiol was verified by TLC (silica gel, *n*-hexane) and by $^1$H NMR (499.84 MHz) and/or $^{13}$C NMR (125.70 MHz) spectroscopy (*i.e.* 40 mg of $C_{18}$S/Au colloid in 0.7 mL of $d_6$-benzene).[1] The $^1$H and $^{13}$C NMR signals of $C_{18}$S chains bound to the Au nanoparticles are considerably broadened as compared to those of free $C_{18}$SH. The $\alpha$, $\beta$, and $\gamma$ methylene proton signals at ~2.5, ~1.6, and ~1.4 ppm, respectively, are not observable for the $C_{18}$S/Au nanoparticles.[1] The solution-state $^{13}$C NMR spectrum is characterized by broad peaks at 13.9 (C18), 22.7 (C17), 31.9 (C16), 30.9 (C4−C14), and 29.5 ppm (C15). The $^{13}$C resonances due to C1, C2, and C3 are not observed for the Au-tethered $C_{18}$S chains.[1,2] With 1.8 mmol of $AuCl_4^-$ as the starting material, 350−380 mg of purified $C_{18}$S/Au powder was obtained.

**Transmission Electron Microscopy.** Samples for TEM were prepared by dipping standard carbon-coated (200−300 Å), Formvar-covered copper grids (200 mesh) into a dilute hexane solution of the RS/Au nanoparticles for several seconds. The TEM grids were withdrawn from the solution and allowed to dry under ambient atmosphere for 5 min. Phase contrast images were obtained with a top-entry Phillips EM 410T electron microscope operated at an accelerating voltage of 80 keV. Micrographs were obtained at magnifications of $6 \times 10^4$ and $8 \times 10^4$. The size distributions of the $C_{18}$S/Au nanoparticles were determined from the diameters of at least 250 particles located in a representative region of the micrographs using a video image analysis software program (SigmaScan Pro3, Jandel Scientific). The particle sizes obtained are the following: *1,1-*$d_2$-$C_{18}$S/Au 27 ± 8 Å; *10,10,11,11,12,12,13,13-*$d_8$-$C_{18}$S/Au 29 ± 8 Å; $d_{35}$-$C_{18}$S/Au 27 ± 6 Å.

**Infrared Spectroscopy.** The $C_{18}$S/Au colloidal particles were deposited dropwise onto a KBr disc from a concentrated hexane solution. Evaporation of the solvent resulted in a uniform film. Infrared spectra were acquired using a Perkin-Elmer FT-IR Microscope Model 16PC (MCT detector) equipped with a Mettler FP 52 hot stage for variable-temperature experiments (10−100 °C). Spectra were collected in the transmission mode with an unpolarized beam, at a resolution of 2 cm$^{-1}$ with 128 scans, and a spectral window of 4000−600 cm$^{-1}$. The IR sample was purged continuously with dry nitrogen and maintained at each temperature for 20 min before a spectrum was acquired. Background spectra of the clean KBr disc were collected at the same temperatures and subtracted from the sample spectra.

**Differential Scanning Calorimetry.** DSC experiments were conducted with a Perkin-Elmer DSC-7 instrument calibrated for temperature and peak area by means of indium and octadecane standards for the −40 to 100 °C temperature range or indium and cyclohexane for runs of −100 to 100 °C. Thermograms were run on samples of ~10 mg of $C_{18}$S/Au particles in sealed aluminum pans under a purging atmosphere of either nitrogen (−40 to 100 °C) or helium (−100 to 100 °C) gas at heat-cool rates of 5 or 10 °C/min.

**Solid-State $^2$H NMR Spectroscopy.** Samples for $^2$H NMR were prepared by packing a shortened 5-mm NMR tube with 150−180 mg of dry $^2$H-labeled $C_{18}$S/Au powder and sealing the tube with Teflon tape. $^2$H NMR spectra were recorded on a Chemagnetics 300-MHz spectrometer operating at a frequency of 46.045 MHz. A quadrupole echo sequence $(90°_{\pm x}-\tau_1-90°_y-\tau_2)$[37] with transmitter blanking was employed and a 500-kHz spectral window was scanned. $\tau_1$ and $\tau_2$ were 40 and 20 $\mu$s, respectively. Spectra were acquired at both low and high temperature with pulse delays ranging from 0.5 to 5 s. Since the longer pulse delay times produced spectra that were identical to the ones acquired using short delays, all spectra were acquired with a pulse delay of 0.5 s to shorten the acquisition time. Depending on the signal-to-noise ratio, between 512 and 29 000 transients were accumulated. After data accumulation, the FID was left-shifted by the correct number of points so that for each spectrum, the FID was Fourier transformed starting at the echo maximum. Heating and cooling of the NMR sample was accomplished using air, cooled by passage through an acetone/dry ice bath, and a calibrated temperature control unit (Chemagnetics). A 30 min sample equilibration time was allowed at each temperature before the start of spectral acquisition. For each $^2$H-labeled $C_{18}$S/Au sample, an initial spectrum was acquired at 25 °C and then spectra were collected at progressively lower temperatures. The cooled sample was then gradually reheated past 25 °C and spectra were collected at higher temperatures. After heating past the melting transition, the sample was cooled to 25 °C and a spectrum was acquired to check if any thermally-induced changes had occurred.

## Results and Discussion

**DSC Measurements.** The phase behavior of thiol-derivatized Au nanoparticles has been characterized by DSC in terms of the temperature and the enthalpy of the phase transition.[1,5] The DSC thermograms clearly show that the RS/Au particles (where R = $C_{12}$−$C_{20}$), in the solid state, undergo distinct phase transitions which can be associated with reversible disordering of the alkyl chains.[1] Both the peak maximum temperature and the enthalpy associated with the DSC transition were found to increase with increasing chain length.[1,5] This trend strongly parallels that seen in other materials undergoing gel-to-liquid crystalline transitions, such as diacylphospholipid vesicles. In fact, the DSC peak maximum temperature and enthalpy measured for $C_{12}$S/Au, $C_{14}$S/Au, $C_{16}$S/Au, and $C_{18}$S/Au are very close to the main transition temperature and enthalpy of *n*-diacylphosphatidylcholines of equivalent chain length.[1,5,38] A comparison[5] to the thermotropic behavior of pure hydrocarbons is not appropriate since the enthalpies of the RSH-derivatized

(37) Davis, J. H.; Jeffrey, K. R.; Bloom, M.; Valic, M. I.; Higgs, T. P. *Chem. Phys. Lett.* **1976**, *42*, 390−394.

(38) The DSC peak maximum temperatures measured for the RS/Au colloids[1] *vs* the DSC peak maximum temperature measured for *n*-diacylphosphatidylcholines[13] of equivalent chain length (value in parentheses) are the following: $C_{12}$, 3 °C (−1.1 ± 0.4 °C),; $C_{14}$, 22 °C (23.5 ± 0.4 °C); $C_{16}$, 41 °C (41.4 ± 0.5 °C); $C_{18}$, 51 °C (55.1 ± 1.5 °C), and $C_{20}$, 64 °C (64.5 ± 0.5 °C). The enthalpies measured for the RS/Au nanoparticles[1,5] in kJ per mol of RS chains *vs* the enthalpies reported for the gel-to-liquid crystalline transitions of *n*-diacylphosphatidylcholines[13] (value given in parentheses in kJ per mol per chain) are the following: $C_{12}$, 6.4 ± 2.5 (6.1 ± 3.4); $C_{14}$, 10 (12.4 ± 1.4); $C_{16}$, 13.8 ± 0.8 (17.4 ± 1.6); and $C_{18}$, 21 (21.2 ± 1.8). A melting temperature of 7 °C (280 K) and an enthalpy of 20 kJ per mol of thiol molecules have been predicted for $C_{12}$S/Au nanoparticles from caloric curves produced by MD simulations.[17]

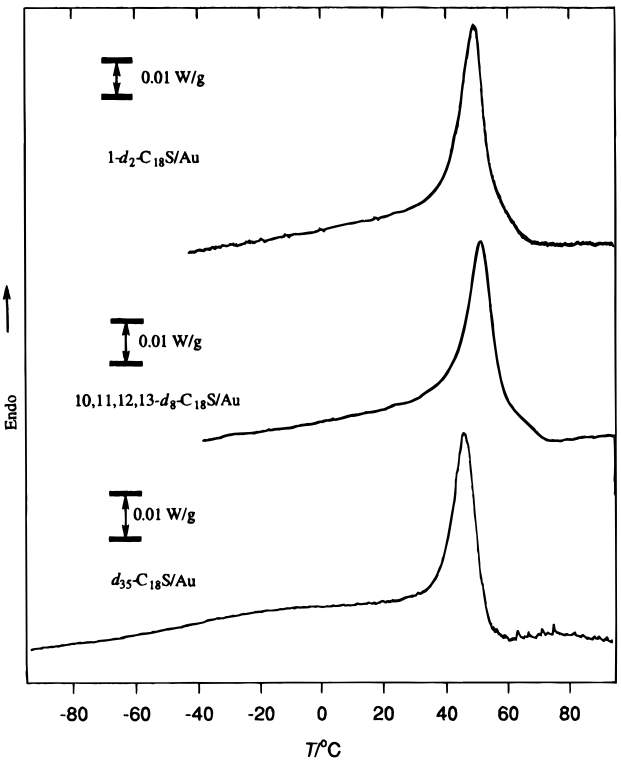


**Figure 1.** DSC endotherms of *1,1-*$d_2$-$C_{18}$S/Au, *10,10,11,11,12,12,13,13-*$d_8$-$C_{18}$S/Au, and $d_{35}$-$C_{18}$S/Au powders. Scan rate is 5 °C·min$^{-1}$ for *1,1-*$d_2$-$C_{18}$S/Au and 10,11,12,13-$d_8$-$C_{18}$S/Au and 10 °C·min$^{-1}$ for $d_{35}$-$C_{18}$S/Au.

Au nanoparticles[38] are much smaller than the melting heats reported for pure alkanes.[39,40] Instead, the alkyl chains are clearly in a gel state, as in lipid membranes, rather than the crystalline state found in pure hydrocarbons.

Figure 1 shows the DSC endotherms of the various deuterated $C_{18}$S/Au samples. The peak maximum temperature for both the *1,1-*$d_2$-$C_{18}$S/Au and $d_{35}$-$C_{18}$S/Au is 48 °C, while the peak maximum temperature for the *10,10,11,11,12,12,13,13-*$d_8$-$C_{18}$S/Au is 52 °C. A peak maximum temperature of 51 °C was previously reported for the fully hydrogenated $C_{18}$S/Au.[1] The main phase transition temperatures of perdeuterated phospholipids[26] are depressed by ∼4−5 °C compared to the fully hydrogenated analogue. Such a definite conclusion cannot be made in our case for the $d_{35}$-$C_{18}$S/Au because the peak maximum temperature observed by DSC varies by 2−3 °C from one RS/Au preparation to another.

It is important to note that whereas the gel-to-liquid crystalline transitions in lipid bilayer membranes occur over *ca*. 5 °C, the transition for the RS/Au colloidal system is relatively broad and occurs over a *ca*. 30 °C temperature range for each sample. Furthermore, the DSC peaks of the deuterated $C_{18}$S/Au samples are preceded by a sloping or curved baseline extending down to −100 °C, which is best seen in the endotherm of $d_{35}$-$C_{18}$S/Au (Figure 1). This may reflect either the existence of a disordered liquid-like chain population or the occurrence of chain motional processes which accompany the phase transition. As suggested earlier, the broadness of the transition may be caused by poor bulk crystallization of the RS/Au nanoparticles.[1,2] Recrystallization and thermal annealing do not however significantly sharpen the DSC peak. The broad transition may also be due to the fairly large particle size distribution which can affect the alkyl chain packing. While these factors can contribute somewhat to the peak broadening, a possible effect of the restricted chain mobility (due to covalent bonding of the sulfur to the Au) on the phase transition must also be considered.

In recent years, model polymer membranes have been designed to obtain lipid bilayers which exhibit thermal stabilities superior to those of biomembranes.[41−43] Such stable membranes are of interest for studies of cell−cell interaction and as drug carriers. For this purpose, a $C_{18}$ diacyl lipid analogue has been synthesized with a polymerizable methacryloylic moiety attached to the quaternary ammonium head group.[41−43] Polymerization restricts the lateral mobility of the lipid head group in the bilayer and is reported to significantly reduce the cooperativity of the gel-to-liquid crystalline phase transition. This restricted head group mobility causes the polymer membrane to exhibit a broader gel-to-liquid crystalline transition than the monomer membrane (*i.e.* the peak width at half maximum is 0.7 °C for the monomer membrane and 2.1 °C for the polymer membrane).[42] Furthermore, the peak maximum temperature is depressed by 20 °C and the enthalpy is reduced by a factor of 2 compared to the monomer bilayer.[42] As mentioned earlier, the DSC peak maximum temperatures and enthalpies measured for $C_{12}$S/Au, $C_{14}$S/Au, $C_{16}$S/Au, and $C_{18}$S/Au nanoparticles are however close to the values of the main transition for *n*-diacylphosphatidylcholine lipids. Thus, even though these lipid molecules have relatively unrestricted lateral mobility whereas pinning of the sulfur to the Au is expected to restrict the alkanethiolate chain mobility, there is no effect manifested in terms of either the RS/Au transition temperature or enthalpy. Melting of the RS/Au nanoparticles also introduces the possibility that rotational and/or lateral motion of the entire particle sets in. The onset of an isotropic peak in the $^2$H NMR spectra at higher temperatures (*vide infra*) may suggest rotation or tumbling of the entire Au particle. MD simulations of $C_{12}$S/Au nanoparticles in fact predict that these clusters have high surface mobilities at temperatures above $T_m$, with a calculated surface diffusion constant ($1.5 \times 10^{-5}$ cm$^2$/s) which is close to that of bulk liquid alkanes.[17] The simulations also show that the diffusive motion of the particles occurs through coupled lateral rotation and translation ("pivoted-slip").[17] This rotation can be formally equivalent to the 2D diffusion available to lipid molecules on melting. If this were the case, then the DSC peak broadness may be a manifestation of the particle size distribution in an indirect way. That is, the particle tumbling rates may be size dependent. The alkyl chains (in this model) must melt before the tumbling (or entropy) issue becomes important. The width of the RS/Au DSC peak and the similarity in the enthalpy values of the RS/Au nanoparticles and *n*-diacylphosphatidylcholine multilamellar vesicles are sensitive indicators of the cooperative nature of the order−disorder process.[44] As such, the broad transitions observed for both planar and colloidal RS/Au SAMs are most probably due to the complex interrelationship between the particle and RS chain domain sizes and their polydispersities.

Bloom and Bayerl also report significant differences in the DSC phase behavior of single lipid bilayers supported on glass microspheres (SSVs) as compared to multilamellar lipid vesicles (MLVs).[26] For instance, the SSV does not exhibit a chain tilt/untilt pretransition, the main transition temperature is lowered

(39) The melting points and enthalpies for pure hydrocarbons are the following: $C_{12}H_{26}$, −9.6 °C (36.6 kJ/mol); $C_{14}H_{30}$, 5.9 °C; $C_{16}H_{34}$, 18.2 °C; $C_{18}H_{38}$, 28.2 °C (61.4 kJ/mol).[40]

(40) *CRC Handbook of Chemistry and Physics*, 70th ed.; Weast, R. C., Ed.; CRC Press, Inc.: Boca Raton, FL, 1989−90.

(41) Ebelhauser, R.; Spiess, H. W. *Makromol. Chem., Rapid Commun.* **1984**, *5*, 403−411.

(42) Ebelhauser, R.; Spiess, H. W. *Ber. Bunsenges. Phys. Chem.* **1985**, *89*, 1208−1214.

(43) Ebelhauser, R.; Spiess, H. W. *Makromol. Chem.* **1987**, *188*, 2935−2949.

(44) Blume, A. *Biochemistry* **1980**, *19*, 4908−4913.

by 2 °C over that of the MLV, the half-width of the main transition peak is a factor of 4 broader for the SSV than for the MLV, the enthalpy of the main transition is 25% lower for the SSV, and the hysteresis observed between the melting and crystallization temperature values is larger.[26] Bloom and Bayerl attribute these changes to *quasi*-2D melting phenomena. In MLVs, interbilayer interactions also increase the cooperativity of the phase transition. This is interesting because fatty acid Langmuir−Blodgett (LB) monolayers on silicon wafers also show broad chain disordering transitions as detected by electron diffraction.[12] The gradual chain disordering occurs over a *ca.* 20 °C temperature range and the temperatures are very similar to those of equivalent chain length RS/Au SAMs.[1] Since the fatty acid chains are only physisorbed to the underlying silicon, the gradual chain melting process observed for these L−B monolayer films cannot be a manifestation of restricted chain mobility due to strong head group−substrate interaction. Thus, it may well be that the broad chain order−disorder phase transitions observed for self-assembled alkanethiol monolayers on planar and colloidal Au surfaces are due to melting in *quasi*-2D systems.

**FT-IR Spectroscopy.** DSC establishes that a phase transition occurs in alkanethiol monolayers self-assembled at colloidal Au surfaces. Although the transition can be characterized in terms of temperature, enthalpy, and cooperativity, no direct information can be obtained from DSC about the conformational state of the alkyl chains. FT-IR spectroscopy is a powerful technique for probing the conformations and orientations of alkyl chains adsorbed to surfaces.[45−51] In particular, the frequencies of the methylene symmetric and antisymmetric vibrational stretches are known to be related to the population of *trans* and *gauche* conformers.[25,46,47,49,52] Variable-temperature transmission FT-IR spectroscopic studies show that these alkylated nanoparticles undergo a transition from a highly chain-ordered state to a chain-disordered state at the phase transition temperatures measured by DSC.[1] However, no insight was gained concerning where the disordering starts in the alkyl chain and how far along the chain the disorder propagates. FT-IR studies of deuterated lipids in multilamellar vesicles[52] and supported on spherical microbeads[25] have shown that the temperature dependence of the symmetric $CD_2$ stretching vibration depends on the average number of *gauche* conformers per lipid acyl chain. The symmetric $CD_2$ stretching frequency (∼2090 $cm^{-1}$) increases by ∼5 $cm^{-1}$ during the gel-to-liquid crystalline phase transition.[25] The antisymmetric $CD_2$ stretch (∼2190 $cm^{-1}$) also increases with temperature, but the shift is less pronounced.[52] By deuterating the $C_{18}SH$ molecule at specific sites along the chain, the thermally-induced onset of local disorder can be monitored *via* the $CD_2$ stretching vibrations.

Figure 2 tracks the $CD_2$ symmetric ($\upsilon_{sym}(CD_2)$) and antisymmetric ($\upsilon_{asym}(CD_2)$) stretches of the deuterated $C_{18}S$/Au samples as a function of temperature. In Figure 3A, the peak position of $\upsilon_{sym}(CD_2)$ is plotted as a function of temperature for $d_{35}$-

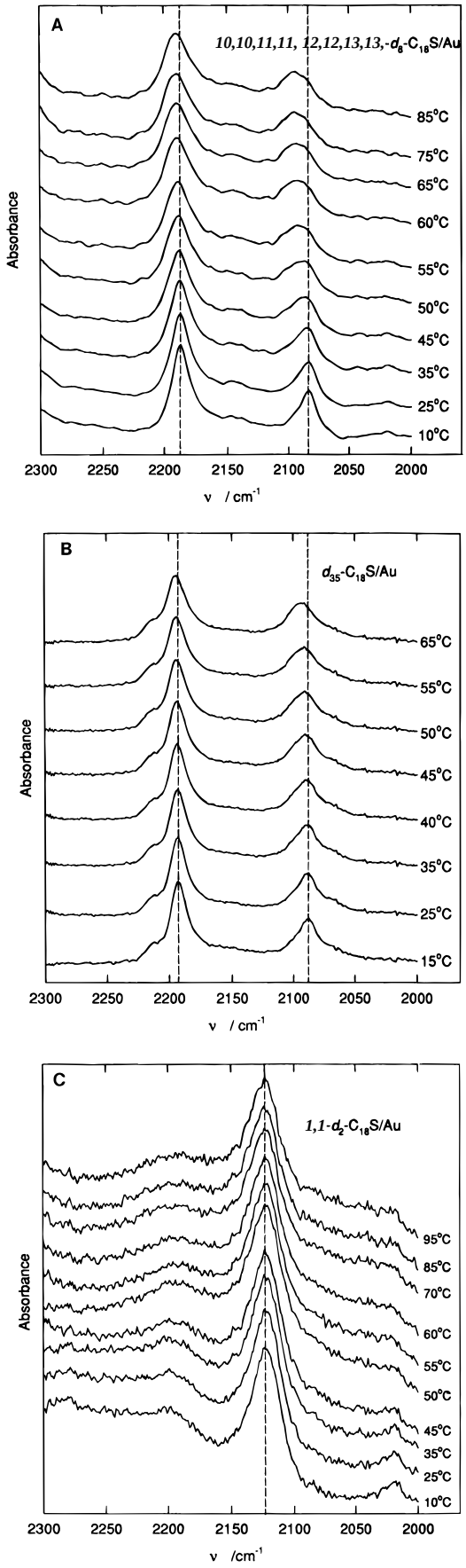


**Figure 2.** Variable-temperature transmission FT-IR spectra of the $CD_2$ stretching region (2300−2000 $cm^{-1}$) for the deuterated $C_{18}S$/Au nanoparticles; (A) *10,10,11,11,12,12,13,13-*$d_8$-$C_{18}S$/Au synthesized using $^1/_3$ labeled $C_{18}SH$ and $^2/_3$ unlabeled $C_{18}SH$, (B) $d_{35}$-$C_{18}S$/Au, and (C) *1,1-*$d_2$-$C_{18}S$/Au. The dotted lines are visual aids.

(45) Porter, M. D.; Bright, T. B.; Allara, D. L.; Chidsey, C. E. D. *J. Am. Chem. Soc.* **1987**, *109*, 3559−3568.
(46) Nuzzo, R. G.; Korenic, E. M.; Dubois, L. H. *J. Chem. Phys.* **1990**, *93*, 767−773.
(47) Dubois, L. H.; Zegarski, B. R.; Nuzzo, R. G. *J. Electron Spectrosc. Relat. Phenom.* **1990**, *54/55*, 1143.
(48) Nuzzo, R. G.; Dubois, L. H.; Allara, D. L. *J. Am. Chem. Soc.* **1990**, *112*, 558−569.
(49) Bensebaa, F.; Ellis, T. H.; Badia, A.; Lennox, R. B. *J. Vac. Sci. Technol. A* **1995**, *13*, 1331−1336.
(50) Ulman, A. *Adv. Mater.* **1991**, *3*, 298−303.
(51) Naselli, C.; Rabolt, J. F.; Swalen, J. D. *J. Chem. Phys.* **1985**, *82*, 2136−2140.
(52) Mendelsohn, R.; Davies, M. A.; Brauner, J. W.; Schuster, H. F.; Dluhy, R. A. *Biochemistry* **1989**, *28*, 8934−8939.

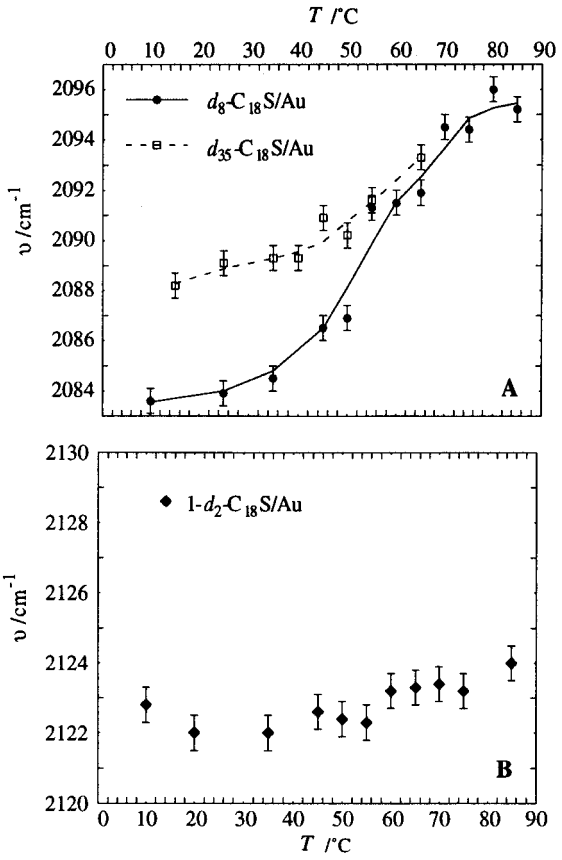


**Figure 3.** The peak position of the symmetric $CD_2$ stretch as a function of temperature for (A) 10,11,12,13-$d_8$-$C_{18}$S/Au and $d_{35}$-$C_{18}$S/Au and (B) *1,1*-$d_2$-$C_{18}$S/Au. The error bars represent a 0.5-$cm^{-1}$ uncertainty in the peak position values.

$C_{18}$S/Au and *10,10,11,11,12,12,13,13*-$d_8$-$C_{18}$S/Au. The value of the $\upsilon_{sym}(CD_2)$ peak frequency for the *10,10,11,11,12,12,13,13*-$d_8$-$C_{18}$S/Au nanoparticles exhibits a sharp discontinuity at the DSC detected phase transition temperature, ~50 °C. By contrast, the $d_{35}$-$C_{18}$S/Au sample shows only a gradual chain disordering transition. A similar trend is observed for the $\upsilon_{asym}(CD_2)$ peak. Furthermore at 10−15 °C, $\upsilon_{sym}(CD_2)$ for *10,10,11,11,12,12,13,13*-$d_8$-$C_{18}$S/Au occurs at ~2084 $cm^{-1}$, while $\upsilon_{sym}(CD_2)$ for $d_{35}$-$C_{18}$S/Au is ~2088 $cm^{-1}$. This clearly indicates that at 10−15 °C, the population of *gauche* conformers is larger in the perdeuterated $C_{18}$S/Au material than for *10,10,11,11,12,12,13,13*-$d_8$-$C_{18}$S/Au. Obviously, in $d_{35}$-$C_{18}$S/Au, there are contributions from *gauche* $CD_2$s located in the $C_{14}$-$C_{17}$ region, even 35 °C below the DSC-detected phase transition temperature. Helium diffraction[53,54] and surface IR studies[46,47] of long-chain alkanethiol SAMs on planar Au confirm that *gauche* conformational defects are concentrated at the chain termini at temperatures below 27 °C. These chain end *gauche* defects persist even at −73 °C.[46,47] Thus, the *ca.* 4-$cm^{-1}$ shift in peak frequency of the symmetric $CD_2$ stretch ($\upsilon_{sym}$) of $d_{35}$-$C_{18}$S/Au relative to that of *10,10,11,11,12,12,13,13*-$d_8$-$C_{18}$S/Au is definitely a result of the disordered state of the chain ends. Since only a gradual shift in $\upsilon_{sym}(CD_2)$ is observed for $d_{35}$-$C_{18}$S/Au with increasing temperature, it is most probable that a weighted average of the *trans* and *gauche* bond populations along the *entire* chain length is reported in this experiment. In variable-temperature surface IR studies of planar alkanethiol monolayers, Dubois and Nuzzo[46,47] observed the gradual appearance of *gauche* conformational chain defects upon heating, instead of the dramatic population increase expected from a first-order melting process. By contrast, the shift in $\upsilon_{sym}(CD_2)$ for $d_8$-$C_{18}$S/Au shown in Figure 3A specifically reflects the temperature dependence of the *trans* and *gauche* bond population at positions 10−13 (*i.e.* in the middle of the alkyl chain) and a sharp transition is observed. Molecular dynamics simulations of $C_{15}$S chains absorbed onto a Au(111) surface in fact predict that at 27 °C, the percentage *gauche* defect concentration is approximately 4.4% and that all of the *gauche* defects are located at the chain termini.[55] At this temperature, the middle of the chain is predicted to be essentially defect free. The FT-IR results described here for *10,10,11,11,12,12,13,13*-$d_8$-$C_{18}$S/Au and $d_{35}$-$C_{18}$S/Au confirm this prediction. As the temperature is raised past 27 °C in the MD calculations, the development of *gauche* bonds is concentrated to the middle of the $C_{15}$S chains and a low *gauche* defect population is observed near the sulfur head group.[55] These predictions are, again, in excellent agreement with the thermal behavior observed here for *10,10,11,11,12,12,13,13*-$d_8$-$C_{18}$S/Au and *1,1*-$d_2$-$C_{18}$S/Au (*vide infra*).

The variable-temperature FT-IR spectra of *1,1*-$d_2$-$C_{18}$S/Au nanoparticles (Figure 2C) show a $\upsilon_{sym}(CD_2)$ peak (~2123 $cm^{-1}$) which is shifted by ~15 $cm^{-1}$ compared to the bulk thiol (~2139 $cm^{-1}$). A weak, broad $\upsilon_{asym}(CD_2)$ peak at *ca.* 2200 $cm^{-1}$ is also observed and represents a shift of ~20 $cm^{-1}$ from that of *1,1*-$d_2$-$C_{18}$SH.[56,57] Interestingly, SERS[58] studies of planar RS/Au SAMs report a *ca.* 20 $cm^{-1}$ decrease in the $\upsilon$(C−S) frequency upon bonding of the thiol to the Au surface due to weakening of the C−S bond. Besides the *ca.* 15-$cm^{-1}$ shift in the $\upsilon_{sym}(CD_2)$ peak observed for the carbon adjacent to the sulfur head group, it is important to note that its position does not shift over the temperature range of 10−90 °C (Figure 3B). This strongly suggests that local order is maintained at the carbon closest to the Au surface during the chain disordering transition described above.

Transmission FT-IR spectroscopy thus definitively establishes that the DSC-detected phase transition arises from an alkyl chain disordering process which increases the number of *gauche* conformers in the chain. One can envisage that specific deuteration along the length of the alkanethiol chain will allow one to study the onset of chain disordering at highly-defined regions in an assembly of alkyl chains.

**$^2$H NMR Spectroscopy.** IR spectroscopy probes molecular vibrations occurring on a time scale shorter than $10^{-10}$ s, so that the IR measurement is essentially a "snapshot" of the different bond conformations existing at a given instant averaged

(53) Chidsey, C. E. D.; Liu, G.-Y.; Rowntree, P.; Scoles, G. *J. Chem. Phys.* **1989**, *91*, 4421−4423.

(54) Camillone, N.; Chidsey, C. E. D.; Liu, G.-Y.; Putvinski, T. M.; Scoles, G. *J. Chem. Phys.* **1991**, *94*, 8493−8502.

(55) Mar, W.; Klein, M. L. *Langmuir* **1994**, *10*, 188−196.

(56) (a) It is noteworthy that for the bulk *1,1*-$d_2$-$C_{18}$SH, the $\upsilon_{asym}(CD_2)$ peak is less intense than the $\upsilon_{sym}(CD_2)$ peak, while in the $d_{35}$-$C_{18}$SH, the $\upsilon_{asym}(CD_2)$ peak is more intense than the $\upsilon_{sym}(CD_2)$ peak. The assignment of the 2120-$cm^{-1}$ peak in the spectrum of *1,1*-$d_2$-$C_{18}$S/Au to $\upsilon_{sym}(CD_2)$ is reasonable since (i) there are no interfering C−H or C−C vibrations in the 2000−2300-$cm^{-1}$ region, (ii) deuteration is at a single position, and (iii) given the relative intensities of the symmetric and antisymmetric $CD_2$ stretches in bulk *1,1*-$d_2$-$C_{18}$SH. Refer to the spectra included in the Supporting Information. (b) The complementary $\upsilon(CH_2)$ data (2800−3000 $cm^{-1}$) for $d_{35}$-$C_{18}$S/Au (*i.e.* hydrogenated at carbon 1) contain significant contributions from CHD due to a 2% isotopic hydrogen impurity.[57] For the $C_{18}$ chain, there are 0.7 CHD and 2 $CH_2$ groups per molecule. These isolated CHD groups cause site-group splitting of the C−H stretches so that no direct comparison can be made with the peak frequencies of fully hydrogenated $C_{18}$S/Au. Refer to the spectra included in the Supporting Information. No site-group splitting of the C−H stretches is however observed for *10,10,11,11,12,12,13,13*-$d_8$-$C_{18}$S/Au due to the insignificant amount of isolated CHD groups (<0.001) compared to $CH_2$ groups (29).

(57) MacPhail, R. A.; Strauss, H. L.; Snyder, R. G.; Elliger, C. A. *J. Phys. Chem.* **1984**, *88*, 334−341.

(58) Bryant, M. E.; Pemberton, J. E. *J. Am. Chem. Soc.* **1991**, *113*, 8284−8293.

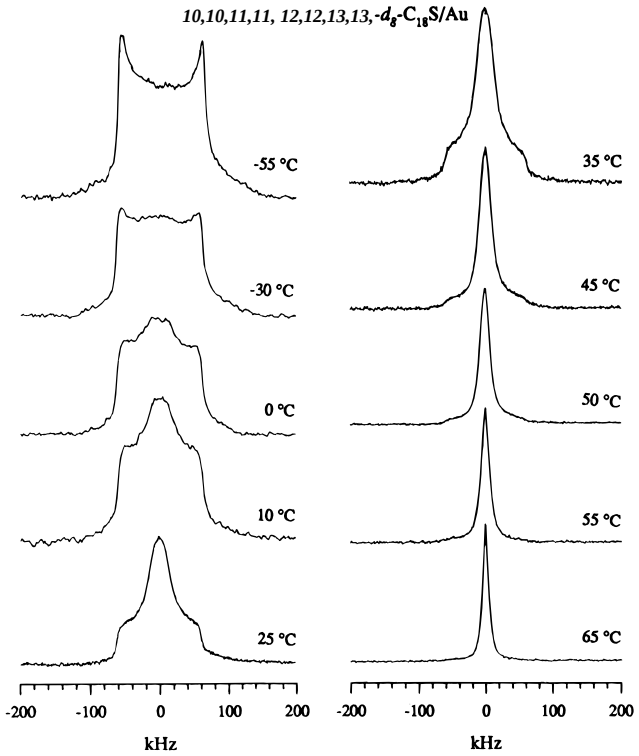


**Figure 4.** $^2$H NMR spectra of *10,10,11,11,12,12,13,13-d*$_8$-$C_{18}$S/Au.

out over the area of irradiation.[35] IR spectroscopy thus reveals the equilibrium *trans* and *gauche* bond populations as a function of temperature, but does not provide any insight about the motional processes which accompany chain disordering. For this reason, the long time scale probed by $^2$H NMR (typically $10^{-6}-10^{-4}$ s)[35] has been exploited to study the temperature dependence of the alkanethiolate chain dynamics.

The variable-temperature $^2$H NMR spectra of *10,10,11,11,12,12,13,13-d*$_8$-$C_{18}$S/Au are displayed in Figure 4. At −55 °C, a static Pake pattern with a quadrupolar splitting of 118 kHz is observed, clearly indicating that there is little motion of the C−$^2$H bonds at positions 10−13 of the bound $C_{18}$S chain. As the *10,10,11,11,12,12,13,13-d*$_8$-$C_{18}$S/Au sample is heated, the $^2$H NMR spectra exhibit motional averaging of the line shape. At −30 °C, the $^2$H resonance appears as a "flat-topped" peak, a line shape which has been attributed to a slow, restricted *trans-gauche* bond isomerization.[33,59,60] Figure 4 shows that with further increases in temperature, a number of the $C_{18}$S chains exhibit a motion that is characterized by rounded triangular patterns such as that observed in the $^2$H NMR spectrum at 0 °C. In the temperature range of *ca.* 0 to 50 °C, the spectral line shapes consist of a narrower triangular component superimposed on a much broader component. The "de-Paked" spectrum at 25 °C (Figure 5), for example, clearly shows that the complex line shape of the powder pattern actually consists of two sets of two peaks. The outer set of peaks has a static quadrupolar splitting of 240 kHz (*i.e.* $\theta = 0°$) and the inner set has a quadrupolar splitting of ∼40 kHz. The inner set of peaks reflects disordered RS chains that are not subject to true isotropic motion because they are tethered to the Au surface. More importantly, with increasing temperature, the relative contribution of the triangular peak increases. The full width at half height (fwhh) of the broad spectral component in the powder pattern is plotted as a function of temperature in Figure 6. The graph reveals that from −55 to 45 °C, the fwhh remains fairly constant at 110−130 kHz. Around the phase transition temperature of 50 °C, the broad component abruptly disappears and the $^2$H NMR spectra at 55 and 65 °C exhibit solely a narrow isotropic peak. The *gauche* conformer population largely determines the width of the broad spectral component.[42] More precisely, when the *gauche* bond population equals the *trans* population, no quadrupole splitting remains.[42] This detail clearly explains the disappearance of the broad spectral component in the $^2$H NMR spectrum between 50 and 55 °C. (Figure 4). The absence of a narrow isotropic peak at temperatures below the phase transition temperature supports our previous suggestion that the chains exist in ordered domains or bundles and that the Au particles close-pack *via* the interdigitation of these ordered chain bundles[1] (Scheme 1). The interdigitation of individual chains on adjacent Au particles would not be sufficient to fill

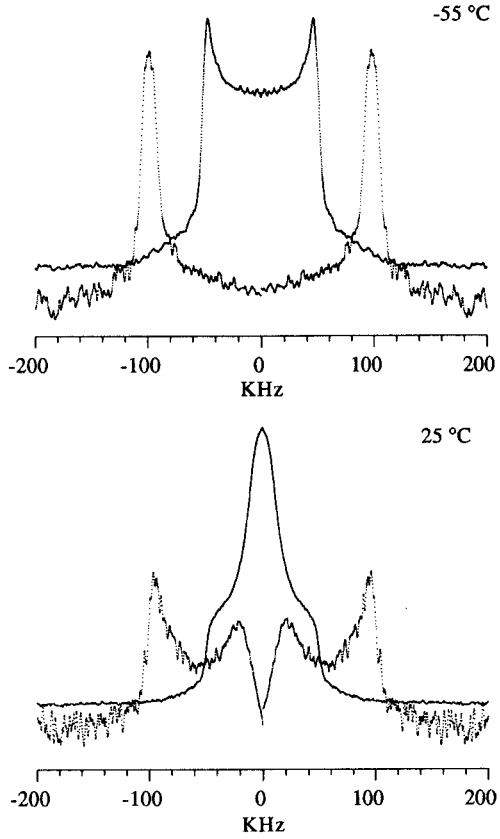


**Figure 5.** Computationally "de-Paked" spectra overlaid on the $^2$H NMR powder patterns obtained at −55 and 25 °C for *10,10,11,11,12,12,13,13-d*$_8$-$C_{18}$S/Au. The "de-Paking" process filters out all but the 0° orientation from the powder pattern.

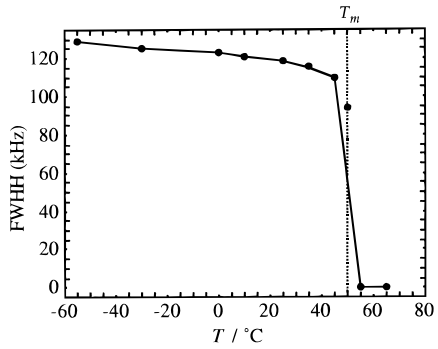


**Figure 6.** Plot of the full width at half height (fwhh) of the broad spectral component in the powder pattern of *10,10,11,11,12,12,13,13-d*$_8$-$C_{18}$S/Au *vs* temperature ($T$). $T_m$ refers to the DSC peak maximum temperature.

(59) Huang, T. H.; Skarjune, R. P.; Witterbort, R. J.; Griffin, R. G.; Oldfield, E. *J. Am. Chem. Soc.* **1980**, *102*, 7377−7379.
(60) Hentschel, D.; Sillescu, H.; Spiess, H. W. *Macromolecules* **1981**, *14*, 1605−1607.

**Scheme 1.** A Schematic 2D Representation of the RS/Au Nanoparticle Packing Structure in the Solid State[a]

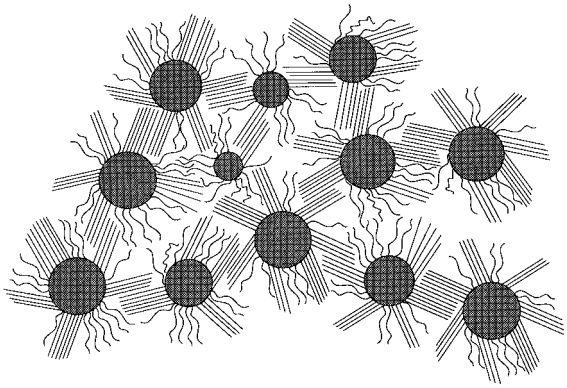

[a] In this description, *domains* or *bundles* of ordered alkylthiolate chains on a given Au particle will interdigitate into the chain domains of neighboring particles in order to compensate for the substantial decrease in the chain density which occurs toward the methyl chain end. Chains with large populations of *gauche* bonds may arise from (i) those which occupy interstitial regions in the particle lattice and cannot efficiently overlap with adjacent chains or from (ii) chains residing at domain boundaries.

the large void volume created by the 14:1 ratio of area available to the chain end to Au−S head group area imposed by the curvature of the nanoparticle. Individually interdigitated chains would be disordered far below the observed phase transition temperature. The $\upsilon(CD_2)$ peak positions (Figures 2 and 3A) observed for *10,10,11,11,12,12,13,13-d*$_8$-$C_{18}$S/Au at *ca.* 35 °C below the phase transition temperature also point to the existence of ordered chain domains.

Both the flat-topped and triangular peak shapes observed in the $^2$H NMR spectra of *10,10,11,11,12,12,13,13-d*$_8$-$C_{18}$S/Au have been observed in studies of amorphous polymers,[33,59,60] liquid crystals,[61] lipid bilayers,[21] polymer model membranes,[41−43] and alkylsilyl-modified silica gel.[32] These line shapes are associated with the conformational exchange of alkyl chains between two unequally populated *trans* and *gauche* sites through the reorientation of individual C−$^2$H bonds around the tetrahedral angle (109.5°). These bond reorientation processes have been modeled using both two-site and six-site "jump" models,[32,33,42,59,61] and the resulting simulated line shapes (*i.e.* flat-topped *vs* triangular peak) are reported to be dependent upon both the relative *trans* and *gauche* bond populations *and* the conformational exchange (or jump) rates. For the RS/Au nanoparticles, the population of *trans* and *gauche* conformers is controlled by the temperature. By analogy to the chain dynamics reported for similar tethered alkyl chain systems,[32,42] a motional model emerges for the RS chains involving both *trans-gauche* bond isomerization and axial chain rotation (Scheme 2).

In this model, the chains are densely packed at temperatures far below the phase transition temperature. Less space is available for molecular reorientations and *trans-gauche* bond isomerization is restricted. This results in a slow conformational exchange rate and the resulting flat-topped spectral line shapes should be describable by a simple two-site jump model.[32,42] A low *gauche* conformer population is expected at these temperatures and the overall orientation of the chains can be maintained by the formation of kinks and jogs.[42] As the number of chain *gauche* conformers increases with temperature, the chain free volume should increase. This causes the pseudo-rotational motion of individual chain segments about the long axis of the

(61) Liesen, J.; Boeffel, C.; Spiess, H. W.; Yoon, D. Y.; Sherwood, M. H.; Kawasumi, M.; Percec, V. *Macromolecules* **1995**, *28*, 6937−6941.

**Scheme 2.** The Types of Chain Dynamic Processes Suggested by the $^2$H NMR Line Shapes of the Deuterated $C_{18}$S/Au Nanoparticles[a]

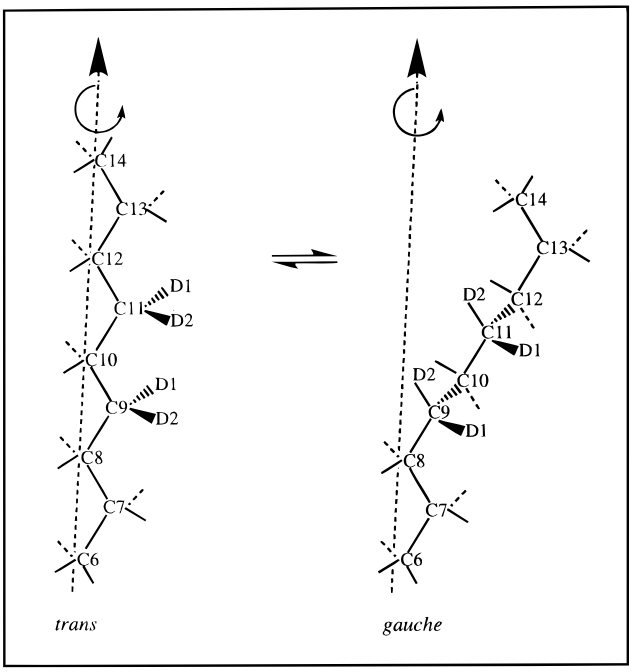


[a] These processes involve *trans-gauche* bond isomerization and pseudorotational motion of individual chain segments about the long axis of the alkanethiolate molecule.

RS molecule.[42] Thus, at higher temperatures, the motional behavior of the RS chain segments is expected to include both axial rotation and rapid bond isomerization, such that the complex, rounded triangular line shapes should be describable by a six-site jump model.[32,42] In fact, molecular dynamics simulations by Mar and Klein[55] predict that the formation of internal *gauche* defects for densely packed $C_{15}$S chains is coupled to the onset of axial chain rotation.[55] Although these qualitative comparisons with the spectral line shapes of other tethered chain systems is insightful, detailed line shape simulations of the $^2$H NMR spectra of *10,10,11,11,12,12,13,13-d*$_8$-$C_{18}$S/Au are presently underway to more precisely define the types and rates of chain motion. At the present time, we are focusing on the broader, qualitative information derived from the temperature dependence of the $^2$H NMR spectra, and not on more refined kinetic information. The latter requires a detailed analysis of the chain conformation kinetics and evolves into issues of model evaluation.

The fact that a rounded triangular peak component is already observed in *10,10,11,11,12,12,13,13-d*$_8$-$C_{18}$S/Au at 0 °C (Figure 4) suggests that there exists a significant population of $C_{18}$S molecules with a large number of *gauche* defects in the middle of the chain at 50 °C below the $T_m$ (DSC peak maximum temperature). This likely arises from a distribution of chain geometries where large *gauche* bond populations exist in chains which occupy interstitial regions in the particle lattice.[1] These chains cannot efficiently interdigitate or bundle with adjacent chains to form ordered domains (Scheme 1). Chains residing at domain boundaries are also expected to be disordered at these low temperatures.[1] In fact, Reven and co-workers have shown through $^{13}$C spin−lattice relaxation measurements of $C_{18}$S/Au that at 25 °C below the $T_m$, a population (74%) of motionally restricted all-*trans* chains coexists with a smaller population (26%) of liquid-like disordered chains.[2] In addition, the $^{13}$C chemical shift of the interior methylene carbons and the reduced methylene $^1$H proton line widths observed in two-dimensional

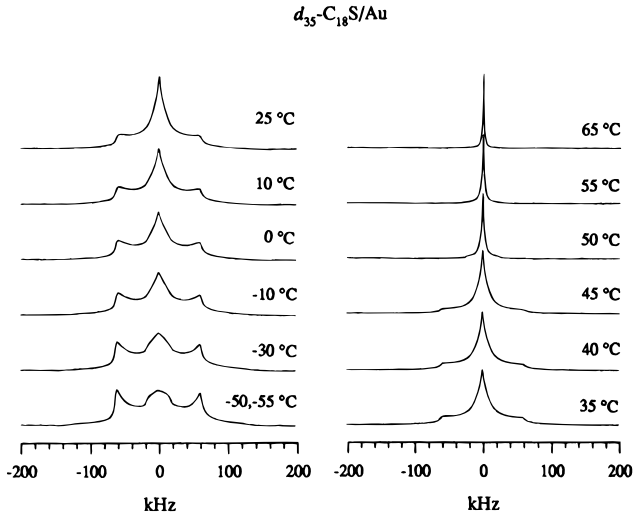


**Figure 7.** $^2$H NMR spectra of $d_{35}$-$C_{18}$S/Au.

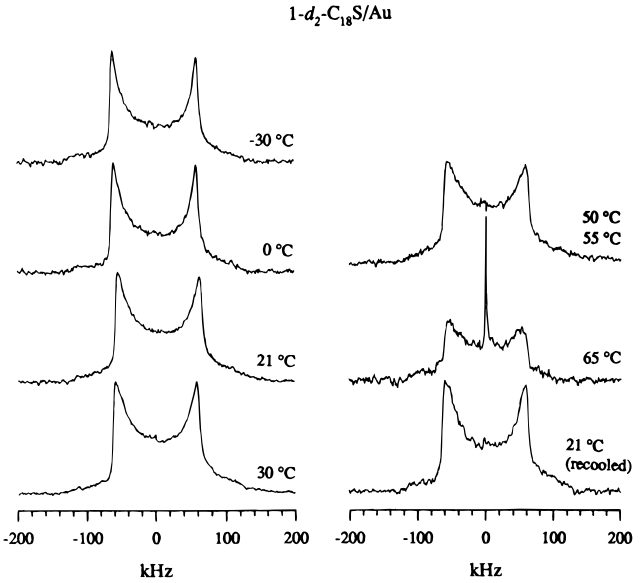


**Figure 8.** $^2$H NMR spectra of *1,1*-$d_2$-$C_{18}$S/Au.

wideline separation (WISE) NMR experiments,[62,63] suggest that the conformationally ordered $C_{18}$S chains are undergoing large-amplitude motions about their long axis at room temperature.[2]

The temperature-dependent behavior of the $^2$H NMR spectra of $d_{35}$-$C_{18}$S/Au (Figure 7) is distinctly different from that of *10,10,11,11,12,12,13,13*-$d_8$-$C_{18}$S/Au, but the spectral line shapes are similar. This suggests that the motions of the chain segments are the same but that their onset occurs at different temperatures for specific regions of the chain. For instance, the spectral line shape of $d_{35}$-$C_{18}$S/Au exhibits a rounded triangular peak in the center of the static Pake pattern at −55 °C (Figure 7). Since *10,10,11,11,12,12,13,13*-$d_8$-$C_{18}$S/Au shows only a rigid Pake pattern at this temperature (Figure 4), the triangular peak must arise from C−$^2$H bond motions at positions 14−18 along the chain. This behavior is expected given that $^{13}$C spin−lattice relaxation measurements[2] indicate that molecular mobility increases toward the untethered chain ends which have a higher population of *gauche* conformers.[46,47,53,54] Moreover, it is in accord with the FT-IR correlations discussed above. It is particularly noteworthy that in contrast to the $^2$H NMR spectra obtained for multilamellar vesicles of perdeuterated lipids,[21,26,37] distinct quadrupolar splittings from individual methylene and methyl resonances are not observed for $d_{35}$-$C_{18}$S/Au. The different splittings observed for the perdeuterated lipids arise from the existence of a flexibility gradient along the lipid chain which changes the characteristics of the molecular motions.[21,22] However, Bayerl and Bloom have shown that as the surface curvature increases for lipid bilayers supported on 0.25-$\mu$m-sized beads (SSVs), the powder spectrum is broadened and the individual methylene quadrupolar splittings become indistinguishable.[26] The RS/Au nanoparticle would contain an extreme case of surface curvature (*i.e.* a radius of 15 Å *vs* 2500 Å in the Bayerl and Bloom SSVs), so that the powder patterns obtained for $d_{35}$-$C_{18}$S/Au most likely reflect the extended chain geometry and large curvature of the metal particle.

It is important to acknowledge that the narrow isotropic peak observed at temperatures above 50 °C ($T = T_m$) for both $d_{35}$-$C_{18}$S/Au and *10,10,11,11,12,12,13,13*-$d_8$-$C_{18}$S/Au may also be associated with rotation or tumbling of the entire Au particle within the ensemble of Au particles. Since the diameter of our Au colloids is the same as the length of the RS chains, Au particle tumbling would presumably be accessible once the alkyl chains have melted, but would not be observable by FT-IR spectroscopy. Further experiments may help to examine this possibility.

Finally, the $^2$H NMR spectra of *1,1*-$d_2$-$C_{18}$S/Au are shown in Figure 8. Unlike, the spectra of *10,10,11,11,12,12,13,13*-$d_8$-$C_{18}$S/Au and $d_{35}$-$C_{18}$S/Au, those of *1,1*-$d_2$-$C_{18}$S/Au are rigid Pake patterns with a quadrupolar splitting of 120 kHz at temperatures up to 65 °C. This establishes that, at least on the microsecond timescale probed by $^2$H NMR spectroscopy: (i) the C1−C2 bond does not experience a measurable degree of *trans-gauche* bond isomerization, (ii) it is unlikely that the alkanethiolate chain undergoes axial rotation about the C−S bond, and (iii) there is no diffusion of the RS−Au species on the Au particle surface. The surface migration of thiolate−Au species has been observed in UHV-STM studies[64−66] over periods of minutes to hours. The rigid Pake patterns observed here for *1,1*-$d_2$-$C_{18}$S/Au do not conclusively reveal whether 2D diffusion of the RS chains, with or without attached Au atoms, occurs on the particle surface. At 65 °C, a narrow isotropic peak is observed in the center of the rigid Pake pattern, whose contribution to the total spectrum is ∼10%. The intensity/contribution of this peak does not change with a further increase in temperature. We believe this isotropic peak is due to melting of free or loosely bound thiol whose motions become isotropic once the entrapping matrix has become disordered.

## Conclusions

RS/Au nanoparticles present themselves as an interesting class of materials given their now obvious parallels to planar SAMs and the fact that their physical properties are strongly dependent upon the structure and properties of the alkanethiolate chains. We have demonstrated in the foregoing that the DSC-detected phase transition is in fact a thermally induced chain melting process. Chain melting begins at the chain terminus region and propagates toward the center of the chain as the temperature increases. FT-IR spectroscopy of specifically deuterated samples establishes that at 35 °C below the calorimetrically-determined phase transition temperature, many of the chain termini are highly disordered while there is a low *gauche* defect density in the middle of the chain and near the sulfur head group. $^2$H

(62) Chin, Y.-H.; Kaplan, S. *Magn. Reson. Chem.* **1994**, S53.
(63) Clauss, J.; Schmidt-Rohr, K.; Adam, A.; Boeffel, C.; Spiess, H. W. *Macromolecules* **1992**, *25*, 5208.
(64) Poirier, G. E.; Tarlov, M. J. *J. Phys. Chem.* **1995**, *99*, 10966−10970.
(65) Bucher, J. P.; Santesson, L.; Kern, K. *Langmuir* **1994**, *10*, 979−983.
(66) Stranick, S. J.; Parikh, A. N.; Allara, D. L.; Weiss, P. S. *J. Phys. Chem.* **1994**, *98*, 11136−11142.

NMR spectroscopy, as a powerful probe of chain order and dynamics, establishes that chain melting arises from an increased frequency of *gauche* bonds in the Au-tethered alkanethiol chains. The excellent correspondence observed between the properties of the planar surface and nanoparticle systems through FT-IR, X-ray diffraction, and calorimetry (differential scanning and electrochemical) experiments suggests that the nanoparticle solid-state NMR ($^2$H and $^{13}$C) conclusions are transferable to the planar RS/Au SAMs.

**Acknowledgment.** The authors wish to thank NSERC (Canada) and FCAR (Quebec) for financial support. This research was funded in part by a Grant-in-Aid of Research from Sigma Xi to A.B. The authors would like to thank Professor Michel Lafleur (Université de Montréal) for providing the dePaking software and for his advice on spectral manipulation. The authors are grateful to Professor Linda Reven (McGill University) for insightful discussions and a critical reading of the manuscript. Professor Royce Murray (University of North Carolina at Chapel Hill) is thanked for providing preprints of his work in this area.

**Supporting Information Available:** Transmission FT-IR spectra (3200−1800 cm$^{-1}$) of bulk $CD_3(CD_2)_{16}CH_2SH$ ($d_{35}$-$C_{18}SH$), $CH_3(CH_2)_{16}CD_2SH$ (*1,1-d*$_2$-$C_{18}SH$), and the corresponding thiol-derivatized Au nanoparticles are given (7 pages). See any current masthead page for ordering and Internet access instructions.

JA963571T